Dyes and Pigments 190 (2021) 109307

Contents lists available at ScienceDirect

Dyes and Pigments

journal homepage: http://www.elsevier.com/locate/dyepig

Redox-responsive nanoparticles self-assembled from porphyrin-betulinic acid conjugates for chemo- and photodynamic therapy

Zulal Özdemir [a,b,1], Mengyao Yang [c,1], Gyoungmi Kim [c], Uladzimir Bildziukevich [a,b], David Šaman [d], Xingshu Li [e,**], Juyoung Yoon [c,*], Zdeněk Wimmer [a,b,***]

[a] Department of Chemistry of Natural Compounds, University of Chemistry and Technology, Prague, Technická 5, 16628, Prague 6, Czech Republic
[b] Isotope laboratory, Institute of Experimental Botany of the Czech Academy of Sciences, Vídeňská 1083, 14220, Prague 4, Czech Republic
[c] Department of Chemistry and Nanoscience, Ewha Womans University, Seoul, 03760, South Korea
[d] Department of NMR Spectroscopy, Institute of Organic Chemistry and Biochemistry of the Czech Academy of Sciences, Flemingovo náměstí 2, 16610, Prague 6, Czech Republic
[e] College of Chemistry, Fuzhou University, Fuzhou, 350108, China

ARTICLE INFO

Keywords:
ROS
Photodynamic therapy
Redox-responsive
Tumour targeting
Self-assembled nanoparticles

ABSTRACT

The redox-responsive nanoparticle (**NanoP-ss-BA**) is designed by linking the porphyrin derivative (**P**) to the naturally occurring betulinic acid (**BA**) through a disulphide bond. A GSH triggered disassembly of **NanoP-ss-BA** effectively promotes a singlet oxygen ($^1O_2$) production, but also releases lipophilic anticancer drug, **BA** *in situ*. Beside this, high phototoxicity of **NanoP-ss-BA** serves it as a good candidate for photodynamic therapy (PDT).

1. Introduction

Conventional chemotherapy agents used for cancer treatment suffer from several limitations including poor bioavailability, nonspecific selectivity, low accumulation in tumours and severe multidrug resistance (MDR) [1]. Photodynamic therapy (PDT) has been recognized as a promising alternative to traditional cancer treatments in clinic [2–4] owing to its spatiotemporal selectivity, wide-spectrum anticancer effect, enabling repeated treatments without initiating resistance and its possible combination with other therapeutic modalities [5–7]. PDT involves exposure of photosensitizer to appropriate wavelength of light which generates short lived, highly cytotoxic reactive oxygen species (ROS), including hydroxyl radical, superoxide ion, hydrogen peroxide and singlet oxygen ($^1O_2$). ROS formed lead to apoptosis and/or necrosis of malignant cells and stimulate the host immune system as well [8]. Besides its advantages, PDT has still many restraints that continues to inspire scientists to overcome the drawbacks of existing protocols. Firstly, low penetration of light through the biological tissues hinders wide applications of PDT for the treatment of deep-seated tumours [9]. Secondly, due to the increased metabolic processes of the destructively proliferating carcinoma cells, the oxygen level of solid tumours is fairly low, therefore outcome from PDT (when it is oxygen-dependent) is quite low, and even worsens during PDT treatment owing to the continuous O_2 depletion (tumour hypoxia) [10]. Lastly, photosensitizers that are "always on" induce undesired skin photosensitization (off toxicity) [11].

To address these limitations, smart nano-photosensitizers that can be prepared *via* a bottom-up strategy have been developed in recent years [5,12,13]. The emergence of nano-photosensitizers not only solves the problems related solubility limitation of hydrophobic drugs, but also increases accumulation of drugs in lesion site [14]. Besides, nano-photosensitizers, being hold by relatively weak noncovalent forces, are usually in a passive state even with light exposure [due to self-assembly process resulting in aggregation-induced quenching (AIQ)] and can be rapidly activated at a target site by various stimuli [15], such as tumour-associated ones [16,17]. Due to high oxidative stress present in tumour tissues, glutathione (GSH) levels are usually

* Corresponding author.
** Corresponding author.
*** Corresponding author. Department of Chemistry of Natural Compounds, University of Chemistry and Technology, Prague, Technická 5, 16628, Prague 6, Czech Republic.
E-mail addresses: xingshuli@fzu.edu.cn (X. Li), jyoon@ewha.ac.kr (J. Yoon), wimmerz@vscht.cz, wimmer@biomed.cas.cz (Z. Wimmer).
[1] Z.Ö. and M.Y. contributed equally.

https://doi.org/10.1016/j.dyepig.2021.109307
Received 11 February 2021; Received in revised form 1 March 2021; Accepted 9 March 2021
Available online 24 March 2021

higher than those in normal tissues and extracellular environments [18,19]. Therefore, GSH level difference present in cellular environment of tumour tissues is one of the approaches that can be exploited for the preparation of activable and stimulus responsive photosensitizers [20–23].

Herein we present a design, development, and therapeutic application of GSH-responsive nanostructure, composed of a hydrophilic photosensitizer, 5,10,15,20-tetrakis(4-carboxy-phenyl)-21*H*,23*H*-porphyrin (**P**) and a lipophilic anticancer agent, betulinic acid [(3β)-3-hydroxylup-20(29) en-28-oic acid (**BA**)] (Scheme 1). Porphyrins, by producing singlet molecular oxygen with high quantum yield upon photoexcitation, continue to play important role in PDT as photosensitizers. Some porphyrins/derivatives have been approved for clinical use [24,25]. **BA** is one of the naturally abundant pentacyclic triterpenoids, secondary plant metabolite, and it was identified as the most promising anticancer agent in a screening of 2500 plant extract [26].

Although **BA** has shown an anticancer activity on a wide range of cancer types [27], it still has some drawbacks such as low water solubility and relatively short half-life, which limits its drug efficacy [28,29]. In our system, conjugation of lipophilic anticancer drug candidate **BA** to hydrophilic **P** through a disulphide bond leads to a formation of a stable dispersion in aqueous solution with a uniform nanosized distribution. This smart prodrug nano-assembly (**NanoP-ss-BA**) is expected to disassemble partially in the presence of high GSH concentration in tumour cells owing to the presence of disulphide bond in its structure. This will enable controlled and targeted release of photosensitizers, which will generate ROS selectively at the site, and consequently, will overcome the drawback of current protocols such as the skin photosensitization (Fig. 1). Concomitantly produced **BA** derivatives will give the **NanoP-ss-BA** a potential to destroy deeply located tumour cells that are out of the PDT range solving another problem related to the tumour hypoxia. Multimodality agent designed here has both imaging and photo-chemo-therapeutic capability to treat the cancer *in vitro*. To our knowledge, **P-ss-BA** is the first conjugate of its type, in which **P** is conjugated to one of the triterpenoid acid (**BA**), mentioned and discussed in the literature [28,29].

2. Results and discussion

Amides **2** and **4** (Scheme 1) were prepared from **BA**, which was converted to its hemisuccinate **1** at the C(3)-OH centre. Because the C(17)-COOH group in **BA** is much less reactive and less accessible than the carboxyl group in the hemisuccinate group, protection of the C(17)-COOH group was not necessary before the subsequent amide bond formation at the hemisuccinate carboxyl group to get **2** and **4**. Amide bonds were constructed by reacting **1** with mono-Boc-protected cystamine and mono-Boc-protected DSOA, using propanephosphonic acid anhydride (T3P) as a carboxylic acid activating reagent; this is a common method described in our earlier papers [30–34]. A removal of the Boc-protecting groups present in **3** and **5** was carried out using 1.0 M HCl in EtOAc, yielding the required compounds **3** and **5**. Amides **3** and **5** were conjugated to **P** by pursuing different strategy than the one mentioned above, because T3P reagent was not successful to construct amide bond between **P** and the respective compounds **3** and **5**.

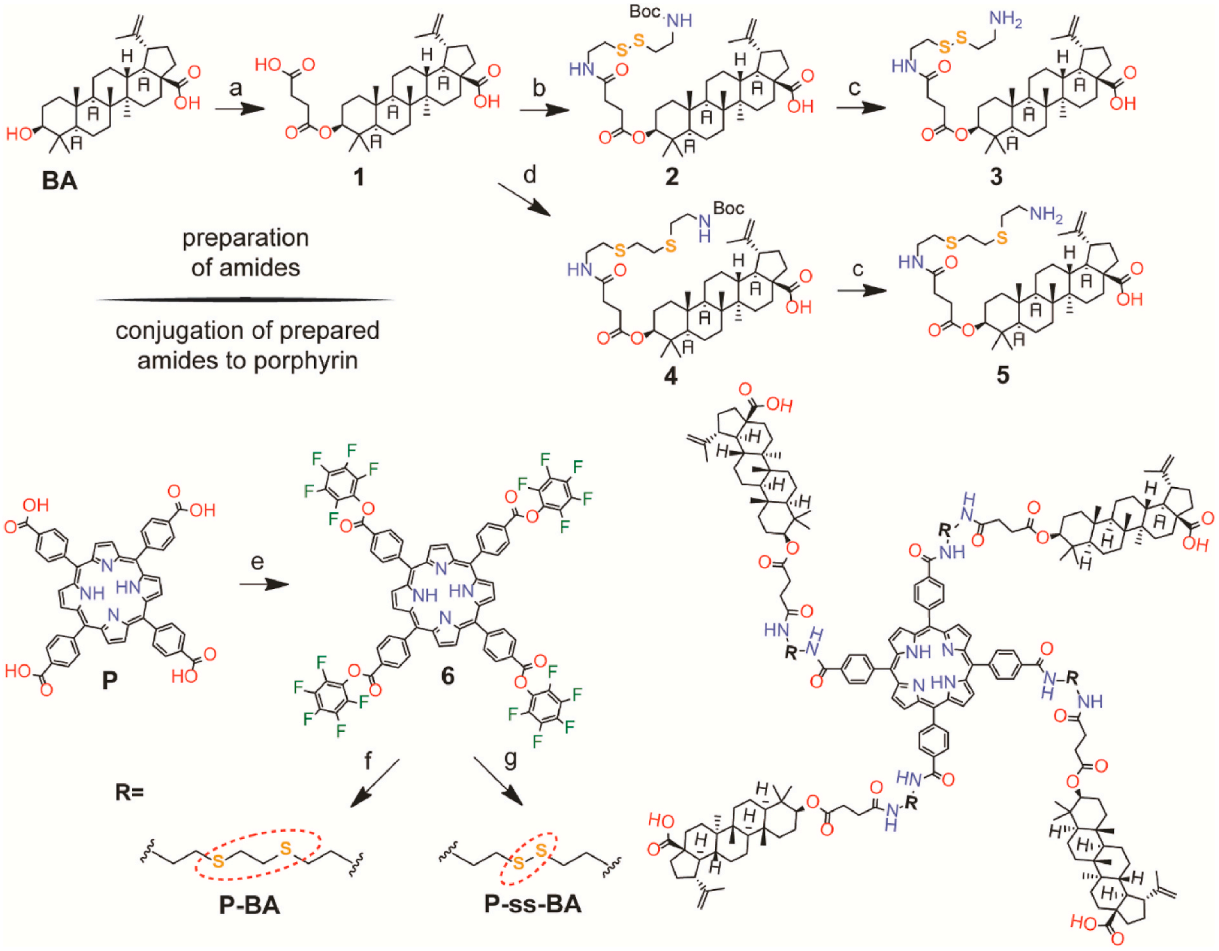

Scheme 1. Synthetic procedure for **P-ss-BA** and **P-BA**. a) succinic anhydride, DMAP, in pyridine, rt b) Boc-cystamine·HCl, T3P (50% in EtOAc), in pyridine, rt; c) HCl (1 M in EtOAc), in dioxane, rt; d) Boc-DSOA·HCl, T3P (50% in EtOAc), in pyridine, rt; e) bis(pentafluorophenyl) carbonate, 4-methylmorpholine, in dimethylformamide (DMF), rt, at dark; f) DIPEA, **3**, in DMF, rt, at dark g) DIPEA, **5**, in DMF, rt, at dark.

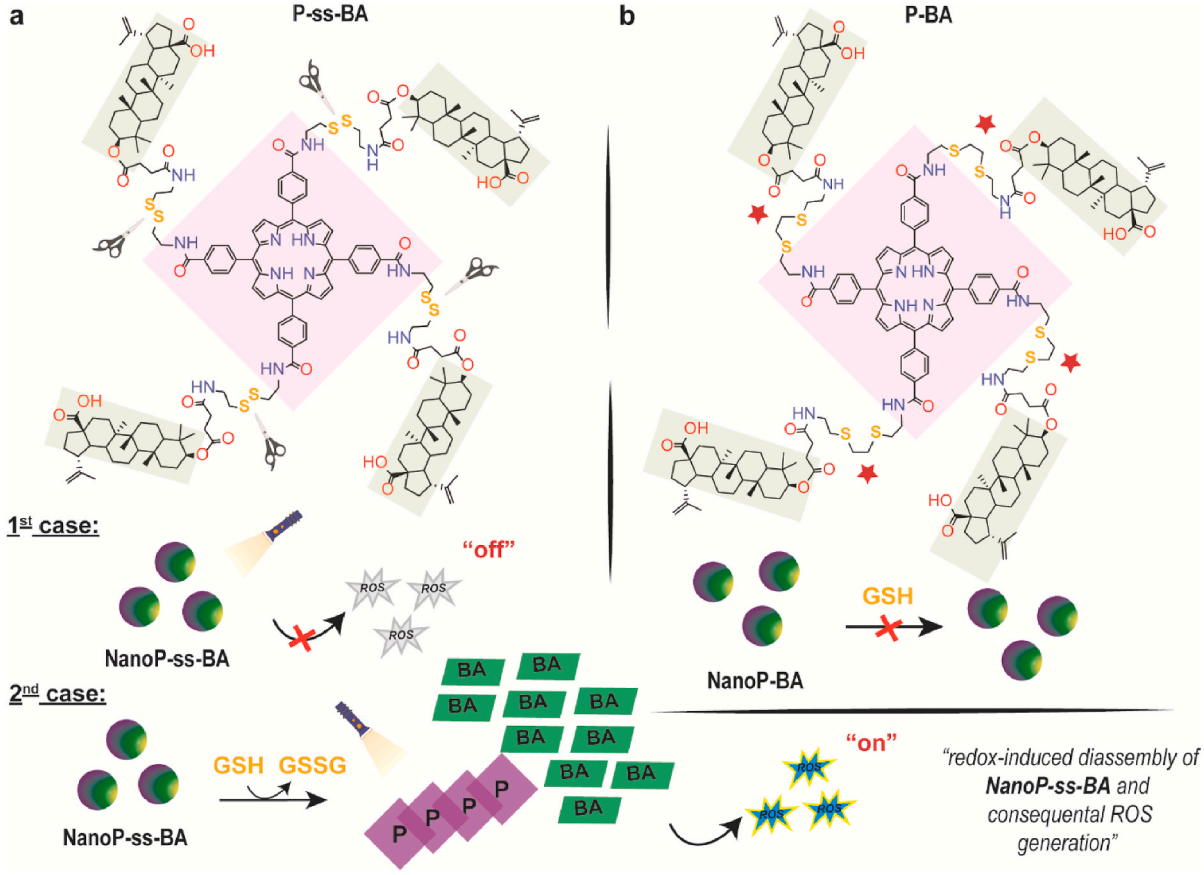

Fig. 1. Structure of a) **P-ss-BA** and b) **P-BA,** and redox-responsive disassembly of **NanoP-ss-BA** and its concomitant PDT effect through a formation of ROS.

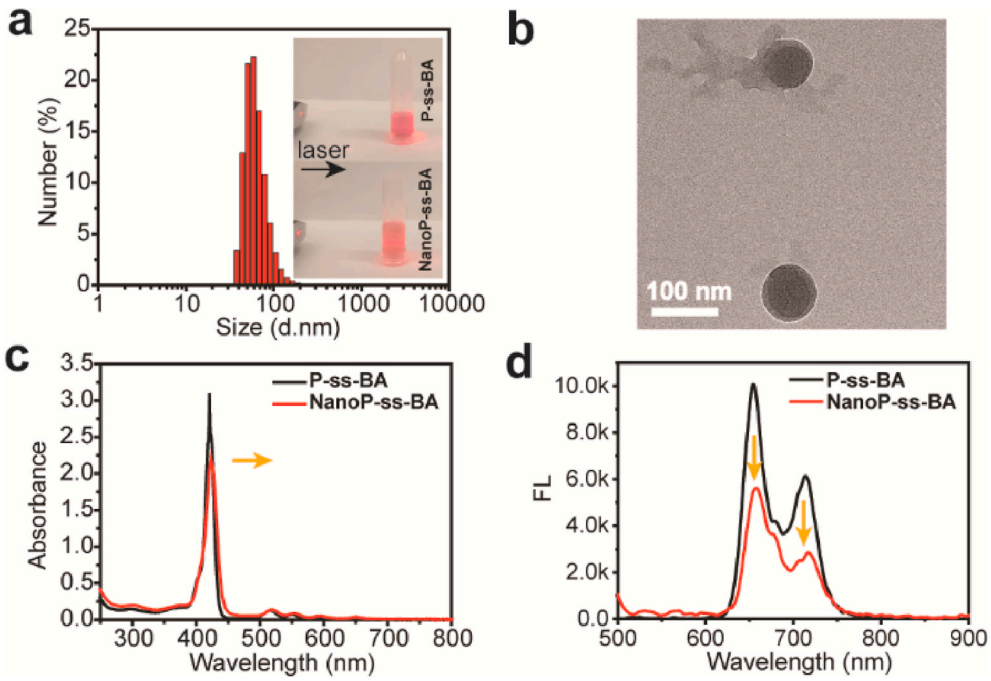

Fig. 2. Characterization of **NanoP-ss-BA** (0.1 mM) assemblies and their photophysical properties. a) Size distribution of **NanoP-ss-BA** in water; b) The morphology of **NanoP-ss-BA** determined by using TEM (0.01 mM); c) Electronic absorption and d) Fluorescence spectra (excited at 420 nm) of **P-ss-BA** in DMSO and **NanoP-ss-BA** in water.

Efforts have been made to improve the reaction outcome by adding DMAP, which is the acyl transfer promoter [35]. However, addition of DMAP did not change the reaction outcome either. Another coupling reagent (*N*,*N*′-diclohexylcarbodiimide; DCC), together with the promotor DMAP, replaced T3P. A formation of 1,3-dicyclohexylurea, a persistent undesired side product during the reaction, and a very low yield of the required products lead us to seek another method again. A conversion of the carboxylic acid groups in **P** to the corresponding acyl chlorides for further coupling with **3** and **5** gave no products, due to high reactivity of the used reagent, oxalyl chloride. Finally, a successful solution was found in a two-step reaction: (a) In the first step, the carboxyl groups of **P** were activated by addition of bis(pentafluorophenyl) carbonate in the presence of 4-methylmorpholine to yield **6**. (b) In the second step, mixing and reacting the activated porphyrin **6** with **3** or **5** furnished **P-ss-BA** or **P-BA**, respectively, in the presence of DIPEA [36].

Size distribution and morphology of nano-assemblies were characterized by dynamic light scattering (DLS) and transmission electron microscope (TEM). As shown in Fig. 2a and Figure S5a (Supplementary data; ESI), **NanoP-ss-BA** and **NanoP-BA** assemblies have an average size of 91.62 and 103.7 nm, and the polydispersity index (PDI) is 0.160 and 0.142 respectively. Inspection of TEM micrograph (Fig. 2b and S5a inlet picture (ESI)) also revealed that both **NanoP-ss-BA** and **NanoP-BA** have regular spherical shapes with an average diameter of about 100 nm. Certain discrepancy in the particle sizes obtained by TEM and DLS techniques may be attributed to the formation of a hydrated layer on the nanoparticles in aqueous system during DLS measurement and shrinkage of nanoparticles occurred as a drying effect during sample preparation for TEM. The size of nanoparticles in the range of 20–200 nm is beneficial to maintain lower level of reticuloendothelial system (RES) internalization, slight renal excretion, and for accumulation of particles in solid tumour through enhanced permeability and retention (EPR) effect [37,38].

Next, the optical properties of the **NanoP-ss-BA** and **P-ss-BA** were compared via UV–vis absorption and fluorescence spectra. The Soret band of **NanoP-ss-BA** at 422 nm, is red-shifted 3 nm and has a lower absorption relative to that of free **P-ss-BA** indicating a formation of *J*-aggregates (Fig. 2c) according to Kasha's exciton theory, thus revealing the head to tail molecular stacking [39] that could be responsible for a formation of **NanoP-ss-BA** assemblies. A presence of *meso*-substituents in the structure that is known to stabilize the *J*-aggregates reinforces this assumption [40]. The fluorescence spectrum indicates that fluorescence emission of **NanoP-ss-BA** in water is slightly quenched, compared to the **P-ss-BA** (Fig. 2d). The exciton delocalization, driven *via* the Forster resonant energy transfer (through the Dexter mechanism), between individual porphyrin cores seems to contribute to fluorescence quenching process [41–43]. Optical properties of **NanoP-BA**, having slight bathochromic shift and fluorescence quenching as well, were similar to that of observed for **NanoP-ss-BA** (See ESI Figure S5b and S5c).

Stability of nanoparticles is an essential criterion when microenvironment of tumour tissue is taken into consideration. Shape and size of nanoparticles should stay the same when they are exposed to physiological medium. Time stability measurements of **NanoP-ss-BA** and **NanoP-BA** in water revealed that their mean sizes do not change significantly after being stored in the dark for 24 h (Fig. 3a and S5d (ESI). The results of the DLS measurement showed that the size and PDI values of diluted **NanoP-ss-BA** and **NanoP-BA** in water remained the same for 24 h (Fig. 3b and S6a (ESI). Optical properties (Fig. 3c and S6b (ESI)) and size distribution of diluted **NanoP-ss-BA** and **NanoP-BA** in 10% foetal bovine serum (FBS) solution (Fig. 3d and S6c (ESI)) are the same as those in water for 24 h suggesting excellent colloidal stability of nano assemblies under the physiological conditions. Lastly, the zeta potentials of **NanoP-ss-BA** and **NanoP-BA** were measured as −22 mV, and −18 mV, respectively. Nanoparticles with a neutral or a negative surface charges usually show reduced adsorption of serum proteins leading to longer-circulation half-lives contrary to those with a positive surface charges [44].

To investigate the effect of GSH on the preformed nano assemblies, several measurements were carried out. DLS results revealed that there is a significant difference in the mean particle diameter and PDI of the **NanoP-ss-BA** assemblies when 3 mM GSH are present in the solution (Fig. 4a). An increase in the particle size and the PDI values of **NanoP-ss-BA** assemblies suggested probable disassembly of discrete particles due to cleavage of the disulphide bond in **NanoP-ss-BA** after addition of GSH (See Table S1, ESI). In the TEM micrograph, reduction-triggered

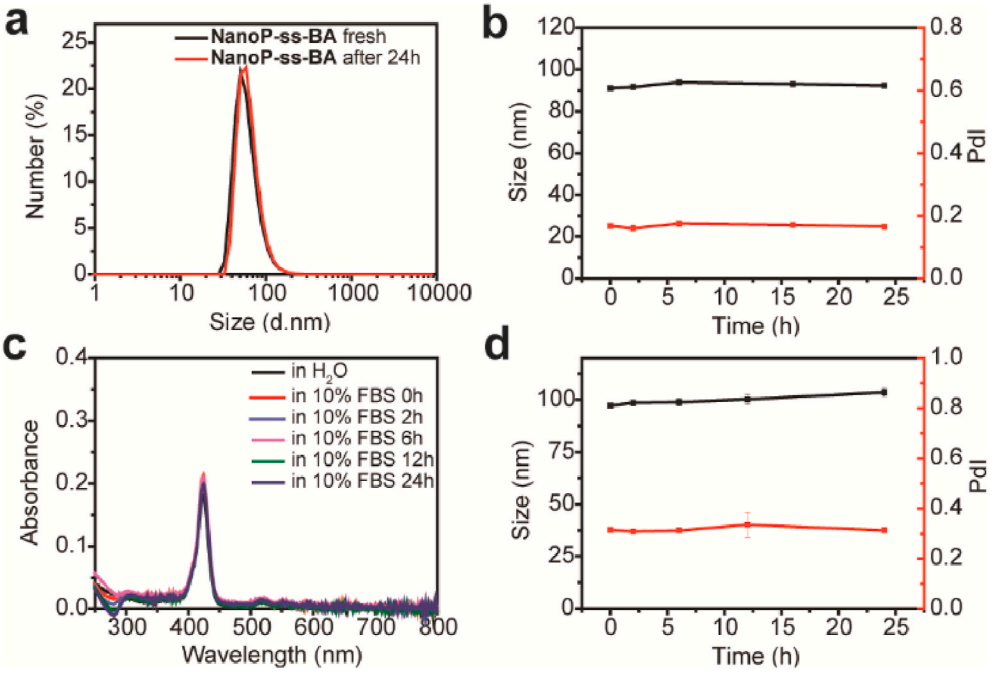

Fig. 3. Stability of **NanoP-ss-BA** assemblies. a) Size distribution of **NanoP-ss-BA** (0.1 mM) in water for 24 h; b) Size and PDI values of **NanoP-ss-BA** (0.01 mM) in water for 24 h; c) Electronic absorption of **NanoP-ss-BA** (0.01 mM) in water and in 10% FBS solution during 24 h; d) Size and PDI values of **NanoP-ss-BA** (0.01 mM) in 10% FBS solution during 24 h.

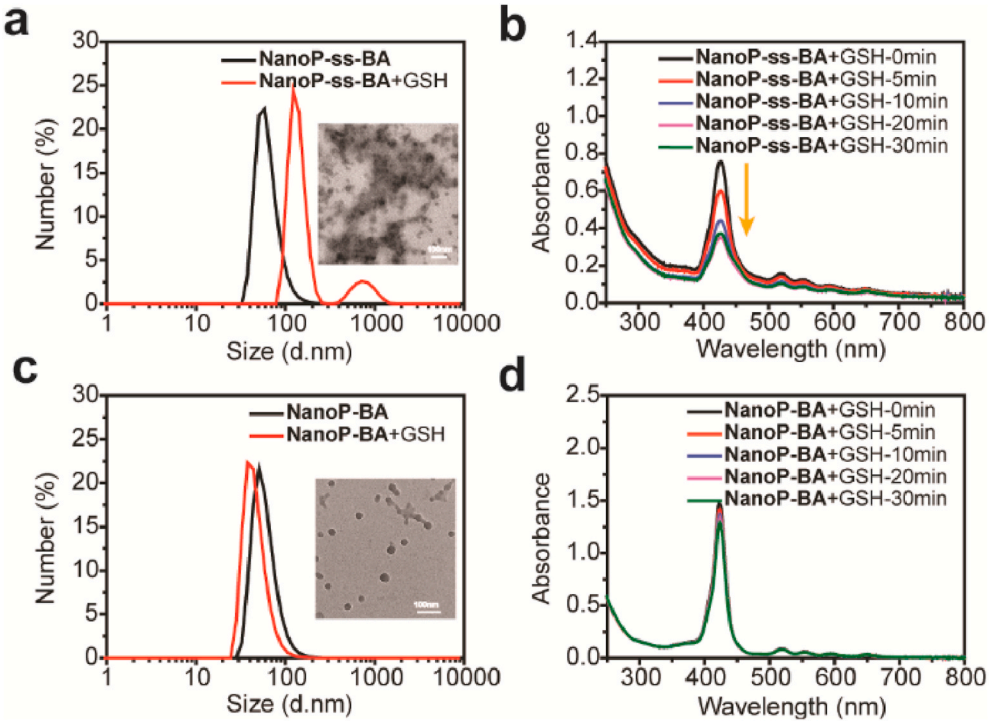

Fig. 4. Effect of GSH on preformed nano-assemblies (0.01 mM). a) DLS data of **NanoP-ss-BA** before and after addition of GSH, inlet picture: TEM micrograph of **NanoP-ss-BA** assemblies after addition of GSH; b) change in electronic absorption spectra of **NanoP-ss-BA** assemblies by time after addition of GSH; c) DLS data of **NanoP-BA** before and after addition of GSH, inlet picture: TEM micrograph of **NanoP-BA** assemblies after addition of GSH; d) change in electronic absorption spectra of **NanoP-BA** assemblies by time after addition of GSH.

destabilization of **NanoP-ss-BA** was detected (Fig. 4a inlet picture, Figure S7, ESI). On the contrary, with **NanoP-BA** assemblies lacking disulphide bond in their structure, addition of GSH did not change their morphology at all (Fig. 4c inlet picture, Figure S7, ESI). Only a slight change in the mean particle diameter and PDI value of **NanoP-BA** assemblies was observed (Fig. 4c and Table S1, ESI). To further support our assumption, electronic absorption spectra of **NanoP-ss-BA** and **NanoP-BA** were compared before and after the GSH addition. While the absorbance intensity of **NanoP-ss-BA** assemblies decreased (Fig. 4b), the absorbance intensity of **NanoP-BA** assemblies remained unchanged (Fig. 4d). The influence of GSH on the photoactivity of the **NanoP-ss-BA** assemblies was also evaluated by investigating their ROS generation capacity, using 9,10-anthracenediyl-bis(methylene)-dimalonic acid (ABDA) as an indicator. While the ROS generation capacity of **NanoP-ss-BA** assemblies are alone low, addition of GSH increased their ROS generation capacity indicating that redox-induced disassembly of nanoparticles enhanced the production of ROS (Fig. 5a) (see ESI Figure S8 for control experiments). As shown in Fig. 5b, absorbance of ABDA decreased by time due to the oxidation of ABDA by the formed ROS. This finding can be explained by "enhanced inter-system crossing"

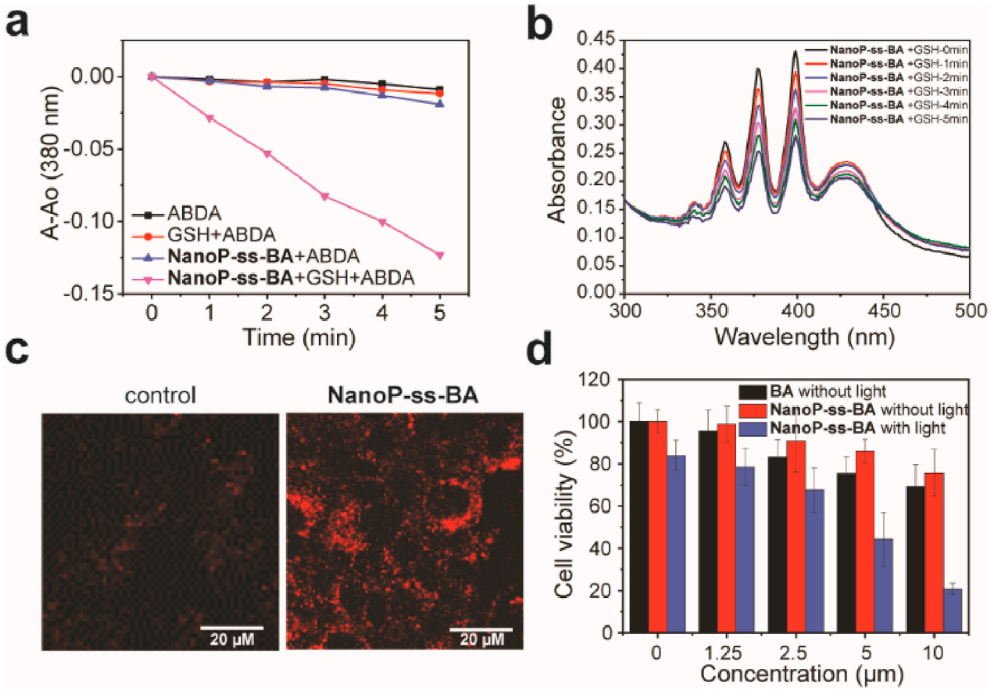

Fig. 5. ROS generation triggered by GSH. a) rate of oxidation of ABDA sensitized by irradiating **NanoP-ss-BA**, **NanoP-ss-BA** + GSH and controls with a halogen lamp, measured by the decrease in the absorption of ABDA at 380 nm as a function of time; b) decrease in the absorption of ABDA sensitized by irritating **NanoP-ss-BA** + GSH; c) CLSM images of 4T1 cancer cells incubated with **NanoP-ss-BA**; d) Dark cytotoxicity of **BA**, **NanoP-ss-BA** and phototoxicity of **NanoP-ss-BA** determined by the MTT assay.

that was probably promoted by a partial disassembly of discrete particles. When the photosensitizer absorbs a photon, this energy can be released generally via three pathways including fluorescence, vibrational relaxation leading to the generation of heat, and intersystem crossing (ISC) leading to a triplet state that promotes generation of ROS [45]. We compared the fluorescence and heat generation of **NanoP-ss-BA** with and without the GSH addition. As shown in Figure S9a, the fluorescence of **NanoP-ss-BA** assemblies decreased by addition of GSH. At the same time, the heat generation of **NanoP-ss-BA** assemblies decreased with the GSH addition as well (Figure S9b). It seems that intersystem crossing mechanism is the most preferred pathway over other two pathways, i.e., disassembly of discrete particles upon addition of GSH promoted intersystem crossing, and, consequently, it led to the improvement of the ROS generation.

To check the efficiency of **NanoP-ss-BA** assemblies in the living cells, additional cell experiments were carried out. Cellular uptake of the **NanoP-ss-BA** assemblies was investigated by a confocal laser scanning microscopy (Fig. 5c). Red fluorescence from **NanoP-ss-BA** indicated that most of the **NanoP-ss-BA** assemblies were internalized in 4T1 cells. Furthermore, the dark cytotoxicity of only **BA**, and the dark and phototoxicity of the **NanoP-ss-BA** assemblies toward cancer cells were evaluated and compared by the MTT assays. **NanoP-ss-BA** without irradiation exhibited similar cytotoxicity with **BA** alone, which is probably due to the release of **BA** in response to the high GSH concentration presents in cellular environment of 4T1. Besides, the viability of 4T1 cells decreased with the increase of **NanoP-ss-BA** concentration under irradiation indicating that **NanoP-ss-BA** exhibited efficient combinational photo- and chemotoxicity towards cancer cells (Fig. 5d). The half-maximal inhibitory concentration (IC_{50}) was determined as 4.25 μM for **NanoP-ss-BA** after irritation with a halogen lamp (0.19 W cm^{-2}, 15 min).

3. Experimental section

3.1. Instrumentation and materials

The ^{1}H NMR and the ^{13}C NMR spectra were recorded on a Bruker AVANCE 600 MHz spectrometer at 600.13 MHz and 150.90 MHz, respectively, in deuterochloroform, unless otherwise stated, using tetramethylsilane ($\delta = 0.0$) as internal reference. The ^{1}H NMR data are presented in the following order: chemical shift (δ) expressed in ppm, multiplicity (s, singlet; d, doublet; t, triplet; q, quartet; m, multiplet), coupling constants in Hertz (Hz), number of protons. Infrared spectra (IR) were measured using a Nicolet 205 FT-IR spectrometer with Attenuated Total Reflection (ATR) method. Mass spectra (MS) were measured with a Waters ZMD mass spectrometer in ESI mode or with an Autoflex Speed MALDI-TOF/TOF mass spectrometer (Bruker Daltonics). Dynamic light scattering (DLS) was measured on a Malvern Zetasizer Nano ZS90 (Malvern Instruments). Transmission electron microscopy (TEM) was carried out with a JEM-2100F transmission electron microscope (JEOL) with a working voltage of 100 kV. All fluorescence measurements were carried out on a FS-2 fluorescence spectrophotometer (Scinco), UV–vis spectra were measured by a Thermo Scientific Evolution 201 UV–Vis spectrophotometer. Thin layer chromatography (TLC) was carried out on silica gel plates (Merck $60F_{254}$; CZ) and the visualization was performed by the ultraviolet (UV) detection and by spraying with the methanolic solution of phosphomolybdic acid (5%) followed by heating. For column chromatography, silica gel 60 (0.063–0.200 mm) from Merck (CZ) was used. All chemicals and solvents were purchased from regular commercial sources in analytical grade and the solvents were purified by general methods before use: betulinic acid (**BA**), Betulinines (Czech Republic; CZ); succinic anhydride (>99%), Aldrich Chemistry (CZ); Boc-cystamine, Iris Biotechnology (Germany; DE)); Boc-DSOA, Iris Biotechnology (DE); 1,4-dioxane, Sigma-Aldrich (CZ); 5,10,15,20-tetrakis(4-carboxyphenyl)-21*H*,23*H*-porphyrin (**P**) (75%), Aldrich Chemistry (CZ); bis(pentafluorophenyl)carbonate (97%), Aldrich Chemistry (CZ); 4-(*N*,*N*-dimethylamino)pyridine (DMAP), (>98%), Fluka (CZ); propanephosphonic acid anhydride (T3P) (50%) in ethyl acetate (EtOAc), Sigma-Aldrich (CZ); hydrogen chloride (HCl) in 1,4-dioxane, 1 M, Acros Organics (Belgium; BE); HCl in EtOAc, 1 M, Acros Organics (BE); *N*,*N*′-dicyclohexylcarbodiimide (DCC) (99%), Fluka (CZ); Diisopropylethylamine (DIPEA) (99%), Sigma-Aldrich (CZ); 4-methylmorfoline (>98%), Fluka (CZ); dimethyl sulfoxide (DMSO), DAEJUNG (Korea; KR); 9,10-Anthracenediyl-bis-(methylene)dimalonic acid (ABDA), Sigma-Aldrich (KR); L-Glutathione reduced (GSH), Sigma-Aldrich (KR).

3.2. Synthesis of the target compounds and their analytical data

3.2.1. (3β)-3-[(3-Carboxypropanoyl)oxy]lup-20(29)-en-28-enoic acid (1)

Succinic anhydride (3.1 g, 31 mmol) and 4-dimethylaminopyridine (0.35 g, 2.9 mmol) were added to a solution of BA (2.2 g, 4.8 mmol) in dry pyridine (20 mL) in a round bottom flask. The mixture was stirred at room temperature for three days. The reaction was monitored using TLC and upon complete conversion of all starting material to product, reaction mixture was poured onto ice, and hydrochloric acid was added to obtain a neutral pH. The reaction mixture was extracted into the chloroform using a separatory funnel. The extract was dried over Na_2SO_4 and filtered. The crude product was column purified on silica gel using mobile phase of regenerated $CHCl_3$/EtOH of lower polarity. The polarity of the mobile phase was gradually increased by 1.0% to afford **1** (2.2017 g) in an 82% yield as a white crystalline solid. ^{1}H NMR (600.13 MHz, $CDCl_3$): δ [ppm] 0.76 (1H, dd, $J_1 = 1.9$ Hz, $J_2 = 11.4$ Hz, H5), 0.80 (3H, s, H23), 0.82 (3H, s, H25), 0.83 (3H, s, H24), 0.91 (3H, s, H26), 0.95 (3H, s, H27), 1.03 (2H, dt, $J_1 = 4.8$ Hz, $J_2 = 13.2$ Hz, $J_3 = 13.2$ Hz, H11), 1.16 (2H, dt, $J_1 = 3.3$ Hz, $J_2 = 3.3$ Hz, $J_3 = 13.8$ Hz, H21), 1.67 (3H, dd, $J_1 = 0.7$ Hz, $J_2 = 1.4$ Hz, H30), 2.14 (1H, ddd, $J_1 = 3.6$ Hz, $J_2 = 11.7$ Hz, $J_3 = 12.8$ Hz, H13), 2.25 (2H, dt, $J_1 = 3.6$ Hz, $J_2 = 3.6$ Hz, $J_3 = 13.1$ Hz, H16), 2.59–2.70 (2H, m, H2′), 2.59–2.70 (2H, m, H3′), 2.97 (1H, dt, $J_1 = 4.9$ Hz, $J_2 = 11.0$ Hz, $J_3 = 11.0$ Hz, H19), 4.49 (1H, dd, $J_1 = 5.4$ Hz, $J_2 = 11.1$ Hz, H3), 4.59 (2H, dq, $J_1 = 1.4$ Hz, $J_2 = 1.4$ Hz, $J_3 = 1.4$ Hz, $J_4 = 2.3$ Hz, H29), 4.71 (2H, dq, $J_1 = 0.7$ Hz, $J_2 = 0.7$ Hz, $J_3 = 0.7$ Hz, $J_4 = 2.3$ Hz, H29). ^{13}C NMR (150.92 MHz, $CDCl_3$): δ [ppm] 14.62 (q, C27), 16.24 (q, C26), 16.29 (q, C25), 16.57 (q, C24), 18.19 (t, C6), 19.33 (q, C30), 20.87 (t, C11), 23.58 (t, C2), 25.34 (t, C12), 28.00 (q, C23), 29.17 (t, C2′), 29.44 (t, C3′), 29.69 (t, C21), 30.53 (t, C15), 32.11 (t, C16), 34.11 (t, C22), 37.05 (s, C10), 37.10 (t, C7), 37.87 (t, C1), 38.21 (s, C4), 38.38 (d, C13), 40.63 (s, C8), 42.37 (s, C14), 46.93 (d, C19), 49.22 (d, C18), 50.18 (d, C9), 55.31 (d, C5), 56.45 (s, C17), 81.51 (d, C3), 109.73 (t, C29), 150.33 (s, C20), 171.67 (s, C1′), 178.11 (s, C4′), 182.58 (s, C28). FT-IR (KBr) ν [cm^{-1}] = 2943 (s) ν(CH) (=CH_2), 2869 (m) ν(CH) (CH_3), 1705 (s) ν(C═O) ester, 1681 (s) ν(C═O) carboxylic acid, 1641 (m) ν(C═C), 1446 (m) $\nu(CH_3)$ $\nu(CH_2)$, 1375 (m) $\nu(CH_3)$ $\nu(CH_2)$, 1270 (m) ν(C–O), 1241 (s) ν(C–O), 1173 (s) ν(C–O), 974 (m), 881 (m), 752 (s), 666 (w), 590 (w), 542 (w), 460 (w), 418 (w). MS (*m*/*z*) = 579.4 $[M+Na]^+$ (ESI^+, coin voltage 20 V), 555.4 $[M-H]^-$ (ESI^-, coin voltage 20 V). For $C_{34}H_{52}O_6$ (556.77) calcd. C 73.34, H 9.41, found C 73.31, H 9.42.

3.2.2. (3β)-3-[(2,2-Dimethyl-4,13,16-trioxo-3-oxa-8,9-dithia-5,12-diazahexadecane-16-yl)oxy]lup-20(29)-en-28-enoic acid (2)

N-Boc-Cystamine·HCl (189 mg, 0.653 mmol) and T3P in EtOAc (50%, 1.2 mL, 2.0 mmol) were added to a solution **1** (400 mg, 0.718 mmol) in dry pyridine (8 mL). The mixture was stirred under argon atmosphere till the next day. Upon complete conversion of all starting material to product, the reaction mixture was extracted into the chloroform ($CHCl_3$) using a separatory funnel (saturated sodium chloride solution was added for better phase separation), dried over anhydrous Na_2SO_4, and the volatiles were removed under reduced pressure. The crude product obtained after aqueous work up was column purified on silica gel using initially petroleum ether (due to its low polarity) in order

to wash off traces of pyridine, followed by $CHCl_3$/ethanol (EtOH) to afford **2** (455 mg) in an 88% yield as a white foam. ^{1}H NMR (600.13 MHz, $CDCl_3$): δ [ppm] 0.82 (1H, dd, $J_1 = 1.8$ Hz, $J_2 = 11.2$ Hz, H5), 0.86 (3H, s, H23), 0.87 (3H, s, H26), 0.89 (3H, d, $J = 0.4$ Hz, H25), 0.98 (3H, s, H24), 1.02 (3H, s, H27), 1.07 (2H, dq, $J_1 = 4.6$ Hz, $J_2 = 13.1$ Hz, $J_3 = 13.1$ Hz, $J_4 = 13.1$ Hz, H2), 1.18 (2H, dt, $J_1 = 3.2$ Hz, $J_2 = 3.2$ Hz, $J_3 = 13.5$ Hz, H21), 1.27 (2H, dq, $J_1 = 4.8$ Hz, $J_2 = 13.0$ Hz, $J_3 = 13.0$ Hz, $J_4 = 13.0$ Hz, H11), 1.43 (9H, s, Boc), 1.70 (3H, dd, $J_1 = 0.7$ Hz, $J_2 = 1.4$ Hz, H30), 2.24 (2H, dt, $J_1 = 3.4$ Hz, $J_2 = 3.4$ Hz, $J_3 = 12.6$ Hz, H16), 2.31 (1H, ddd, $J_1 = 3.6$ Hz, $J_2 = 11.7$ Hz, $J_3 = 12.9$ Hz, H13), 2.50 (2H, t, $J = 6.6$ Hz, H2′), 2.56–2.65 (2H, m, H3′), 2.78 (2H, t, $J = 6.7$ Hz, H6′), 2.81 (2H, t, $J = 6.6$ Hz, H7′), 3.02 (1H, dt, $J_1 = 4.8$ Hz, $J_2 = 10.9$ Hz, $J_3 = 10.9$ Hz, H19), 3.32–3.37 (2H, m, H8′), 3.43–3.51 (2H, m, H5′), 4.46 (1H, dd, $J_1 = 5.1$ Hz, $J_2 = 11.3$ Hz, H3), 4.59 (1H, dq, $J_1 = 1.4$ Hz, $J_2 = 1.4$ Hz, $J_3 = 1.4$ Hz, $J_4 = 2.4$ Hz, H29), 4.71 (1H, dq, $J_1 = 0.7$ Hz, $J_2 = 0.7$ Hz, $J_3 = 0.7$ Hz, $J_4 = 2.4$ Hz, H29). ^{13}C NMR (150.92 MHz, $CDCl_3$): δ [ppm] 15.14 (q, C27), 16.64 (q, C24), 16.77 (q, C25), 17.09 (q, C26), 19.27 (t, C6), 19.55 (q, C30), 22.12 (t, C11), 24.68 (t, C12), 26.83 (t, C2), 28.54 (q, C23), 28.79 (q, Boc), 30.75 (t, C2′), 30.83 (t, C21), 31.40 (t, C3′), 31.70 (t, C15), 33.34 (t, C16), 35.48 (t, C22), 38.14 (t, C1), 38.30 (d, C13), 38.62 (t, C6′), 38.94 (s, C10), 39.07 (t, C7′), 39.57 (t, C7), 39.62 (s, C4), 40.78 (t, C5′), 40.90 (t, C8′), 41.94 (s, C8), 43.61 (s, C14), 48.50 (d, C19), 50.42 (d, C18), 51.87 (d, C9), 56.88 (d, C5), 57.48 (s, C17), 80.18 (s, Boc), 82.62 (d, C3), 110.20 (t, C29), 151.97 (s, C20), 158.41 (s, Boc), 174.09 (s, C1′), 174.39 (s, C4′), 180.07 (s, C28). FT-IR (KBr) ν [cm^{-1}] = 3325 (w, br) ν(NH), 2939 (s) ν(CH) (=CH_2), 2869 (m) ν(CH) (CH_3), 1695 (s, sh) ν(C═O) ester, 1645 (m, sh) ν(C═O) carboxylic acid, 1645 (m, sh) ν(C═O) amide, 1645 (m, sh) ν(C═C), 1508 (sh, m) ν(NH), 1449 (m) ν(CH_3) ν(CH_2), 1364 (s) ν(CH_3) ν(CH_2), 1247 (w) ν(C–O), 1164 (s) ν(C–O), 977 (m), 882 (m), 751 (s), 543 (w), 468 (w) ν(S–S). MS (*m/z*) = 790.9 $[M+H]^+$ (ESI^+, coin voltage 20 V), 788.7 $[M-H]^-$ (ESI^-, coin voltage 20 V). For $C_{43}H_{70}N_2O_7S_2$ (791.46) calcd. C 65.28, H 8.92, N 3.54, S 8.11, found C 65.25, H 8.94, N 3.56, S 8.08.

3.2.3. (3β)-3-{[4-({2-[(2-Aminoethyl)disulphanyl]ethyl}amino)-4-oxobutanoyl]oxy}lup-20(29)-en-28-acid (3)

A solution of HCl in EtOAc (1 M, 15.3 mL, 15.33 mmol) was added to a solution 2 (422 mg, 0.533 mmol) in tetrahydrofuran (THF) (15 mL). The reaction mixture was placed in a shaker at 25 °C and mixed for 10 h. The resulting substance after removal of volatiles under reduced pressure, was column purified on silica gel using $CHCl_3$/EtOH. Then crystallization was carried out in EtOH to afford **3** (89 mg) in a 24% yield as a white crystal. ^{1}H NMR (600.13 MHz, $CDCl_3$): δ [ppm] 0.83 (1H, dd, $J_1 = 2.3$ Hz, $J_2 = 11.8$ Hz, H5), 0.86 (3H, s, H23), 0.87 (3H, d, $J = 0.7$ Hz, H26), 0.89 (3H, s, H25), 0.97 (3H, s, H24), 1.02 (3H, d, $J = 0.5$ Hz, H27), 1.27 (2H, dq, $J_1 = 4.7$ Hz, $J_2 = 13.1$ Hz, $J_3 = 13.1$ Hz, $J_4 = 13.1$ Hz, H2), 1.27 (2H, dq, $J_1 = 4.6$ Hz, $J_2 = 12.8$ Hz, $J_3 = 12.8$ Hz, $J_4 = 12.8$ Hz, H11), 1.70 (3H, dd, $J_1 = 0.7$ Hz, $J_2 = 1.4$ Hz, H30), 2.23 (2H, dt, $J_1 = 3.4$ Hz, $J_2 = 3.4$ Hz, $J_3 = 12.8$ Hz, H16), 2.43 (1H, ddd, $J_1 = 3.6$ Hz, $J_2 = 11.2$ Hz, $J_3 = 13.1$ Hz, H13), 2.49–2.52 (2H, m, H2′), 2.59–2.63 (2H, m, H3′), 2.85 (2H, dt, $J_1 = 0.8$ Hz, $J_2 = 6.8$ Hz, H6′), 2.98 (2H, dt, $J_1 = 0.8$ Hz, $J_2 = 6.8$ Hz, H7′), 3.02 (1H, dt, $J_1 = 4.9$ Hz, $J_2 = 11.0$ Hz, $J_3 = 11.0$ Hz, H19), 3.28 (2H, bt, $J = 6.8$ Hz, H5′), 3.50 (2H, bt, $J = 6.8$ Hz, H8′), 4.47 (1H, dd, $J_1 = 5.1$ Hz, $J_2 = 11.2$ Hz, H3), 4.59 (1H, dq, $J_1 = 1.4$ Hz, $J_2 = 1.4$ Hz, $J_3 = 1.4$ Hz, $J_4 = 2.4$ Hz, H29), 4.71 (1H, dq, $J_1 = 0.7$ Hz, $J_2 = 0.7$ Hz, $J_3 = 0.7$ Hz, $J_4 = 2.4$ Hz, H29). ^{13}C NMR (150.92 MHz, $CDCl_3$): δ [ppm] 15.11 (q, C27), 16.62 (q, C24), 16.75 (q, C25), 17.06 (q, C26), 19.26 (t, C6), 19.54 (q, C30), 22.11 (t, C11), 24.68 (t, C12), 26.82 (t, C2), 28.53 (q, C23), 30.69 (t, C21), 30.82 (t, C3′), 31.37 (t, C2′), 31.68 (t, C15), 33.30 (t, C16), 35.46 (t, C22), 35.51 (t, C6′), 38.11 (t, C1), 38.22 (d, C13), 38.29 (s, C10), 38.94 (t, C7′), 39.38 (t, C5′), 39.55 (s, C4), 39.57 (t, C7), 39.61 (t, C8′), 41.93 (s, C8), 43.59 (s, C14), 48.49 (d, C19), 50.40 (d, C18), 51.87 (d, C9), 56.89 (d, C5), 57.45 (s, C17), 82.63 (d, C3), 110.19 (t, C29), 151.96 (s, C20), 174.12 (s, C1′), 174.53 (s, C4′), 179.96 (s, C28). FT-IR (KBr) ν [cm^{-1}] = 3500–2500 (br) ν(NH^+), 2940 (s) ν(CH) (=CH_2), 2865 (m) ν(CH) (CH_3), 1729 (s) ν(C═O) ester, 1683 (w) ν(C═O) carboxylic acid, 1652 (m, sh) ν(C═O) amide, 1640 (w) ν(C═C), 1539 (m) ν(NH), 1448 (m) ν(CH_3) ν(CH_2), 1362 (s) ν(CH_3) ν(CH_2), 1254 (s) ν(C–O), 1189 (m) ν(C–N), 1150 (m) ν(C–O), 1106 (w), 1006 (m), 979 (s), 878 (m), 793 (w), 633 (w), 570 (w), 543 (w), 471 (m) ν(S–S). MS (*m/z*) = 691.2 $[M+H]^+$ (ESI^+, coin voltage 20 V), 689.0 $[M-H]^-$ (ESI^-, coin voltage 20 V). For C39H64N2O5S2 (705.07) calcd. C 66.44, H 9.15, N 3.97, S 9.10, found C 66.47, H 9.13, N 3.99, S 9.07.

3.2.4. (3β)-3-[(2,2-Dimethyl-4,15,18-trioxo-3-oxa-8,11-dithia-5,14-diazaoctadecane-18-yl)oxy]lup-20(29)-en-28-enoic acid (4)

N-Boc-DSOA·HCl (206.9 mg, 0.653 mmol) and T3P in EtOAc (50%, 3.6 mL, 6.04 mmol) were added to a solution **1** (400 mg, 0.718 mmol) in dry pyridine (8 mL). The mixture was stirred under argon atmosphere overnight. Upon complete conversion of all starting material to product, the reaction mixture was extracted into the $CHCl_3$ using a separatory funnel (saturated NaCl solution was added for better phase separation), dried over anhydrous Na_2SO_4 and the volatiles were removed under reduced pressure. The crude product obtained after aqueous work up was column purified on silica gel using initially petroleum ether (due to its low polarity) in order to wash off traces of pyridine, followed by a $CHCl_3$/EtOH mixture affording **4** (510 mg) in a 95% yield as a white foam. ^{1}H NMR (600.13 MHz, CD_3OD): δ [ppm] 0.82 (1H, dd, $J_1 = 2.2$ Hz, $J_2 = 11.5$ Hz, H5), 0.86 (3H, s, H23), 0.87 (3H, s, H26), 0.89 (3H, d, $J = 0.6$ Hz, H25), 0.98 (3H, s, H24), 1.02 (3H, d, $J = 0.7$ Hz, H27), 1.07 (2H, dq, $J_1 = 4.7$ Hz, $J_2 = 13.2$ Hz, $J_3 = 13.2$ Hz, $J_4 = 13.2$ Hz, H2), 1.18 (2H, dt, $J_1 = 3.3$ Hz, $J_2 = 3.3$ Hz, $J_3 = 13.5$ Hz, H21), 1.26 (2H, dq, $J_1 = 4.5$ Hz, $J_2 = 12.7$ Hz, $J_3 = 12.7$ Hz, $J_4 = 12.7$ Hz, H11), 1.70 (3H, dd, $J_1 = 0.7$ Hz, $J_2 = 1.4$ Hz, H30), 2.23 (2H, ddd, $J_1 = 3.0$ Hz, $J_2 = 3.7$ Hz, $J_3 = 12.9$ Hz, H16), 2.31 (1H, ddd, $J_1 = 3.6$ Hz, $J_2 = 11.5$ Hz, $J_3 = 12.9$ Hz, H13), 2.47–2.51 (2H, m, H2′), 2.59–2.63 (2H, m, H7′), 2.59–2.63 (2H, m, H3′), 2.66 (2H, t, $J = 7.1$ Hz, H6′), 3.02 (1H, dt, $J_1 = 4.8$ Hz, $J_2 = 11.0$ Hz, $J_3 = 11.0$ Hz, H19), 3.20–3.24 (2H, m, H10′), 3.32–3.38 (2H, m, H5′), 4.46 (1H, dd, $J_1 = 5.0$ Hz, $J_2 = 11.4$ Hz, H3), 4.59 (2H, dq, $J_1 = 1.4$ Hz, $J_2 = 1.4$ Hz, $J_3 = 1.4$ Hz, $J_4 = 2.4$ Hz, H29), 4.71 (2H, dq, $J_1 = 0.7$ Hz, $J_2 = 0.7$ Hz, $J_3 = 0.7$ Hz, $J_4 = 2.4$ Hz, H29). ^{13}C NMR (150.92 MHz, CD_3OD): δ [ppm] 15.12 (q, C27), 16.63 (q, C24), 16.76 (q, C25), 17.08 (q, C26), 19.27 (t, C6), 19.54 (q, C30), 22.11 (t, C11), 24.68 (t, C12), 26.83 (t, C2), 28.54 (q, C23), 28.79 (q, C13′), 30.79 (t, C3′), 30.83 (t, C21), 31.45 (t, C2′), 31.70 (t, C15), 32.02 (t, C9′), 32.57 (t, C6′), 32.86 (t, C7′), 32.90 (t, C8′), 33.33 (t, C16), 35.48 (t, C22), 38.13 (t, C1), 38.30 (s, C4), 38.95 (s, C10), 39.57 (t, C7), 39.63 (d, C13), 40.39 (t, C5′), 41.51 (t, C10′), 41.95 (s, C8), 43.61 (s, C14), 48.68 (d, C19), 50.42 (d, C18), 51.87 (d, C9), 56.89 (d, C5), 57.48 (s, C17), 80.12 (s, C12′), 82.63 (d, C3), 110.19 (t, C29), 151.99 (s, C20), 158.36 (s, C11′), 174.10 (s, C1′), 174.29 (s, C4′), 180.05 (s, C28). FT-IR (KBr) ν [cm^{-1}] = 3325 (w, br) ν(NH), 2939 (s) ν(CH) (=CH2), 2869 (m) ν(CH) (CH_3), 1700 (s, sh) ν(C═O) ester, 1654 (m, sh) ν(C═O) carboxylic acid, 1654 (m, sh) ν(C═O) amide, 1654 (m, sh) ν(C═C), 1521 (sh, m) ν(NH), 1448 (m) ν(CH_3) d(CH2), 1364 (s) ν(CH_3) ν(CH_2), 1246 (w) ν(C–O), 1164 (s) ν(C–O), 976 (m), 882 (m), 750 (s), 543 (w). MS (*m/z*) = 819.3 $[M+H]^+$ (ESI^+, coin voltage 20 V), 817.4 $[M-H]^-$ (ESI^-, coin voltage 20 V). For $C_{45}H_{74}N_2O_7S_2$ (819.21) calcd. C 65.98, H 9.10, N 3.42, S 7.83, found C 66.00, H 9.08, N 3.44, S 7.85.

3.2.5. (3β)-3-[(4-{[2-({2-[(2-aminoethyl)sulphanyl]ethyl}sulphanyl)-ethyl]amino}-4-oxobutanoyl)oxy]lup-20(29)-en-28-enoic acid (5)

A solution of HCl in EtOAc (1 M, 5.8 mL, 5.8 mmol) was added to a solution **4** (475 mg, 0.580 mmol) in THF (5 mL). The reaction mixture was placed in a shaker at 25 °C and mixed for 10 h. The resulting residue was filtered using sintered glass funnel and washed with diethyl ether to furnish **5** (353 mg) as a white solid with an 85% yield. ^{1}H NMR (600.13 MHz, CD_3OD): δ [ppm] 0.82 (1H, dd, $J_1 = 2.2$ Hz, $J_2 = 11.4$ Hz, H5), 0.86 (3H, s, H23), 0.87 (3H, s, H26), 0.89 (3H, s, H25), 0.97 (3H, s, H24), 1.02 (3H, d, $J = 0.6$ Hz, H27), 1.07 (2H, dq, $J_1 = 4.7$ Hz, $J_2 = 13.2$ Hz, $J_3 = 13.2$ Hz, $J_4 = 13.2$ Hz, H2), 1.18 (2H, dt, $J_1 = 3.2$ Hz, $J_2 = 3.2$ Hz, $J_3 = 13.5$ Hz, H21), 1.26 (2H, dq, $J_1 = 4.7$ Hz, $J_2 = 12.9$ Hz, $J_3 =$

12.9 Hz, J_4 = 12.9 Hz, H11), 1.70 (3H, dd, J_1 = 0.7 Hz, J_2 = 1.4 Hz, H30), 2.23 (2H, ddd, J_1 = 3.2 Hz, J_2 = 3.7 Hz, J_3 = 13.0 Hz, H16), 2.31 (1H, ddd, J_1 = 3.7 Hz, J_2 = 11.6 Hz, J_3 = 13.0 Hz, H13), 2.48–2.52 (2H, m, J = 7.2 Hz, H2′), 2.57–2.63 (2H, m, H3′), 2.66 (2H, t, J = 7.2 Hz, H6′), 2.77–2.82 (2H, m, H8′), 2.77–2.82 (2H, m, H7′), 3.02 (1H, dt, J_1 = 4.9 Hz, J_2 = 10.9 Hz, J_3 = 10.9 Hz, H19), 3.16 (2H, t, J = 7.0 Hz, H10′), 3.32–3.36 (2H, m, H5′), 4.46 (1H, dd, J_1 = 5.0 Hz, J_2 = 11.3 Hz, H3), 4.59 (2H, dq, J_1 = 1.4 Hz, J_2 = 1.4 Hz, J_3 = 1.4 Hz, J_4 = 2.3 Hz, H29), 4.71 (2H, dq, J_1 = 0.7 Hz, J_2 = 0.7 Hz, J_3 = 0.7 Hz, J_4 = 2.3 Hz, H29). ^{13}C NMR (150.92 MHz, CD_3OD): δ [ppm] 15.11 (q, C27), 16.62 (q, C24), 16.74 (q, C25), 17.07 (q, C26), 19.26 (t, C6), 19.54 (q, C30), 22.11 (t, C11), 24.68 (t, C12), 26.82 (t, C2), 28.54 (q, C23), 29.77 (t, C3′), 30.87 (t, C21), 31.46 (t, C2′), 31.68 (t, C6′), 31.70 (t, C15), 31.84 (t, C9′), 32.43 (t, C8′), 32.53 (t, C7′), 35.46 (t, C22), 36.30 (t, C16), 38.11 (s, C4), 38.29 (t, C1), 38.94 (s, C10), 39.57 (d, C13), 39.62 (t, C7), 40.06 (t, C5′), 40.32 (t, C10′), 41.93 (s, C8), 43.60 (s, C14), 48.49 (d, C19), 50.40 (d, C18), 51.87 (d, C9), 56.88 (d, C5), 57.45 (s, C17), 82.63 (d, C3), 110.19 (t, C29), 151.96 (s, C20), 174.10 (s, C1′), 174.42 (s, C4′), 179.96 (s, C28). FT-IR (KBr) ν [cm^{-1}] = 3500–2500 (br) ν(NH+), 2941 (s) ν(CH) (=CH_2), 2867 (m) ν(CH) (CH_3), 1731 (m) ν(C═O) ester, 1682 (s) ν(C═O) carboxylic acid, 1652 (m, sh) ν(C═O) amide, 1645 (w) ν(C═C), 1540 (w) ν(NH), 1455 (m) ν(CH_3) ν(CH_2), 1376 (m) ν(CH_3) ν(CH_2), 1271 (m) ν(C–O), 1194 (s) ν(C–N), 1106 (w) ν(C–O), 1009 (m), 978 (m), 880 (s), 748 (w), 668 (w), 575 (w), 543 (w), 466 (m) ν(S–S). MS (m/z) = 719.3 $[M+H]^+$ (ESI^+, coin voltage 20 V), 717.2 $[M-H]^-$ (ESI^-, coin voltage 20 V). For $C_{40}H_{66}N_2O_5S_2$ (719.09) calcd. C 66.81, H 9.25, N 3.90, S 8.92, found C 66.79, H 9.26, N 3.92, S 8.95.

3.2.6. Tetrakis(perfluorophenyl)4,4′,4′′,4′′′-(porphyrin-5,10,15,20-tetrayl) tetrabenzoate (6)

4-Methylmorpholine (98%, 57 μL, 0.508 mmol) and bis(pentafluorophenyl) carbonate (97%, 205.5 mg, 0.506 mmol) were added to a solution of 5,10,15,20-tetrakis(4-carboxyphenyl)-21*H*,23*H*-porphyrin (**P**; 75%, 100 mg, 0.126 mmol) in dry DMF (2 mL). The reaction mixture was stirred under argon atmosphere overnight. The reaction was monitored using TLC, and an additional amount of bis(pentafluorophenyl) carbonate (97%, 100 mg, 0.246 mmol) was added. Upon completion of the reaction, DMF was removed under reduced pressure. The crude product obtained after evaporation was column purified on silica gel using petroleum ether in $CHCl_3$ (from 100/0 (v/v) [%] to 2/1 (v/v) [%]) to afford **6** (87 mg) in a 47% yield as a purple powder that was directly used in the next reaction step without isolation.

3.2.7. Synthesis of P-ss-BA

Compound **3** (100 mg, 0.145 mmol) and DIPEA (25.2 μl, 0.145 mmol) were added to a solution of activated porphyrin **6** (47.8 mg, 0.0329 mmol) in DMF (8 mL). The mixture was stirred at r.t. in the absence of light for 4 h. The reaction was monitored using TLC and upon complete conversion of all starting material to product, solvent was evaporated under reduced pressure. The crude product obtained after evaporation was purified by TLC plate using EtOH in $CHCl_3$ (15:1 (v/v) [%]) as a mobile phase to afford **P-ss-BA** (66 mg) in a 58% yield as a dark red powder. ^{1}H NMR (600.13 MHz, DMSO-d_6): δ [ppm] 9.18 (1H, bdd, J_1 = 4.4 Hz, J_2 = 11.0, H3), 1.29 (1H, bt, J_1 = 11.3 Hz, H18), 0.59 (3H, s, H23), 0.22 (3H, s, H24), 0.50 (3H, s, H25), 0.59 (3H, s, H26), 0.62 (3H, s, H27), 1.51 (3H, bs, H30), 4.45 (1H, s, H29), 4.58 (1H, s, H29), 2.40 (2H, t, J = 7.4 Hz, H2′), 2.48–2.52 (2H, m, H3′), 3.07 (2H, bt, J = 6.7 Hz H5′), 3.07 (2H, bt, J = 6.7 Hz H8′), 2.85–2.88 (2H, m, H6′), 2.85–2.88 (2H, m, H7′), 8.26–8.29 (1H, m, H11′), 8.32–8.35 (1H, m, H12′), 8.32 (s, 16H′), 8.23 (1H, bt, J = 6.5 Hz, NH), −2.92 (1H, bs, porph.-NH). ^{13}C NMR (150,92 MHz, DMSO-d_6): δ [ppm] 36.20 (t, C1), 22.95 (t, C2), 79.68 (d, C3), 37.45 (s, C4), 54.40 (d, C5), 17.41 (t, C6), 37.32 (t, C7), 36.30 (s, C8), 49.35 (d, C9), 37.16 (s, C10), 20.09 (t, C11), 24.86 (t, C12), 37.32 (d, C13), 41.74 (s, C14), 31.58 (t, C15), 33.43 (t, C16), 55.28 (s, C17), 48.39 (d, C18), 46.49 (d, C19), 150.26 (s, C20), 29.40 (t, C21), 37.45 (t, C22), 27.44 (q, C23), 15.33 (q, C24), 16.13 (q, C25), 16.13 (q, C26), 14.02 (q, C27), 177.24 (s, C28), 18.83 (q, C30), 109.48 (t, C29), 170.96 (s, C1′), 29.40 (s, C2′), 29.00 (s, C3′), 171.75 (s, C4′), 38.13 (t, C5′), 30.06 (t, C6′), 29.91 (t, C7′), 37.32 (t, C8′), 166.27 (s, C9′), 134.07 (s, C10′), 125.94 (d, C11′), 133.82 (d, C12′), 143.80 (s, C13′), 119.31 (s, C14′), 134.07 (s, C15′), 79.19 (d, C16’). FT-IR (KBr) ν [cm^{-1}] = 3310 (w, br) ν(NH) and pyrrole, 2937 (s) ν(CH) (=CH_2), 2867 (m) ν(CH) (CH_3), 1718 (m) ν(C═O) ester, 1653 (w) ν(C═O) carboxylic acid, 1640 (s, sh) ν(C═O) amide, 1608 (w) ν(C═C), 1522 (s) ν(NH), 1448 (m) ν(CH_3) ν(CH_2), 1362 (m) ν(CH_3) ν(CH_2), 1221 (m) ν(C–O), 1179 (s, br) ν(C–O), 1105 (w) ν(C–N), 966 (s), 881 (m), 799 (m), 750 (s), 668, 543 (w). MALDI MS (m/z) = 3483.19 Da. For $C_{200}H_{270}N_{12}O_{24}S_8$ (3482.87) calcd. C 68.97, H 7.81, N 4.83, S 7.37, found C 68.94, H 7.82, N 4.80, S 7.40.

3.2.8. Synthesis of P-BA

Compound **5** (100 mg, 0.139 mmol) and DIPEA (387.5 μl, 2.22 mmol) were added to a solution of activated porphyrin 6 (46.0 mg, 0.0316 mmol) in DMF (5 mL). The mixture was stirred at r.t. in the absence of light for 3 h. The reaction was monitored using TLC and upon complete conversion of all starting material to product, solvent was evaporated under reduced pressure. The crude product obtained after evaporation was column purified on silica gel using EtOH in $CHCl_3$ (20:1 (v/v) [%] to 15:1 (v/v) [%]) to afford **P-BA** (73 mg) in a 64% yield as dark red powder. ^{1}H NMR (600.13 MHz, DMSO-d_6): δ [ppm] 0.23 (3H, s, H24), 0.50 (3H, s, H25), 0.58 (3H, s, H23), 0.59 (3H, s, H26), 0.64 (3H, s, H27), 1.31 (1H, dt, J = 11.5 Hz, H18), 1.52 (3H, s, H30), 2.35 (2H, t, J = 7.6 Hz, H2′), 2.47–2.49 (2H, m, H3′), 2.62 (2H, t, J = 7.2 Hz, H6′), 2.80–2.91 (2H, m, H8′), 2.80–2.91 (2H, m, H7′), 2.80–2.91 (2H, m, H9′), 3.22–3.28 (2H, m, H5′), 3.62 (2H, dd, J = 5.8 Hz, H10′), 4.18 (1H, dd, J_1 = 4.7 Hz, J_2 = 11.2 Hz, H3), 4.46 (2H, s, H29), 4.47 (2H, s, H29), 8.08 (1H, t, J = 5.8 Hz, H5′-NH), 8.27–8.32 (2H, m, H13′), 8.27–8.32 (2H, m, H14′), 8.27–8.32 (1H, m, H18′), −2.93 (1H, bs, porph.-NH). ^{13}C NMR (150.92 MHz, DMSO-d_6): δ [ppm] 14.04 (q, C27), 15.33 (q, C24), 16.22 12’ (q, C26), 16.33 (q, C25), 17.39 (t, C6), 18.82 (q, C30), 20.05 (t, C11), 22.93 (t, C2), 24.85 (t, C12), 27.43 (q, C23), 29.43 (t, C3′), 29.87 (t, C2′), 30.00 (t, C21), 30.41 (t, C9′), 30.49 (t, C6′), 31.09 (t, C8′), 31.11 (t, C7′), 31.48 (t, C15), 33.40 (t, C16), 36.17 (s, C8), 36.20 (t, C1), 37.33 (s, C10), 37.34 (t, C22), 37.42 (s, C4), 37.56 (t, C7), 38.81 (t, C5′), 41.75 (s, C14), 42.30 (d, C13), 46.45 (d, C19), 48.35 (d, C18), 49.32 (d, C9), 54.37 (d, C5), 55.24 (s, C17), 79.68 (d, C3), 109.53 (t, C29), 119.30 (s, C16′), 125.05 (d, C13′), 133.90 (s, C12′), 133.90 (d, C14′), 134.10 (s, C17′), 143.99 (s, C15′), 150.18 (s, C20), 166.11 (s, C11′), 170.76 (s, C1′), 171.72 (s, C4′), 177.13 (s, C28). FT-IR (KBr) ν [cm^{-1}] = 3307 (w, br) ν(NH) and pyrrole, 2937 (s) ν(CH) (=CH_2), 2864 (m) ν(CH) (CH_3), 1716 (m) ν(C═O) ester, 1645 (s, sh) ν(C═O) carboxylic acid, 1608 (w) ν(C═C), 1526 (s) ν(NH), 1447 (m) ν(CH_3) ν(CH_2), 1363 (s) ν(CH_3) ν(CH_2), 1270 (w) ν(C–O), 1149 (s, br) ν(C–O), 1105 (s, sh) ν(C–N), 966 (s), 882 (w), 799 (s), 749 (s), 667 (w), 458 (s). MALDI MS (m/z) = 3659.88 Da. For $C_{212}H_{302}N_{12}O_{24}S_8$ (3659.25) calcd. C 69.58, H 8.32, N 4.59, S 7.01, found C 69.61, H 8.30, N 4.61, S 6.97.

3.3. Preparation of nano assemblies

NanoP-ss-BA and **NanoP-BA** were obtained by re-precipitation method. Specifically, 100 μL stock solution of **P-ss-BA** or **NanoP-BA** (1 mM in DMSO) was taken, added into water (900 μL) drop by drop, shaken gently, and finally yielded a purple solution of **NanoP-ss-BA** or **NanoP-BA** (0.1 mM). The obtained solutions were aged for 3 h before analysis.

3.4. Redox responsiveness of the nano assemblies

NanoP-ss-BA and **NanoP-BA** (0.01 mM) were incubated with GSH (3 mM) for 30 min, and the GSH responsive behaviour of them was measured, using the UV–vis absorption and fluorescence emission spectra. DLS and TEM were used to measure the changes in the size and

morphology of the **NanoP-ss-BA** and **NanoP-BA** after and before incubation with GSH.

3.5. Redox induced ROS generation of NanoP-ss-BA in a solution

To analyse the influence of redox environment on the photoactivity of **NanoP-ss-BA** nanostructures, **NanoP-ss-BA** (0.01 mM) and GSH (3 mM) were incubated during one day in water. Then, this solution and **NanoP-ss-BA** (0.01 mM) in water were added into a singlet oxygen probe [9,10-anthracenediyl-bis(methylene)dimalonic acid (ABDA)] at a final concentration of 0.02 mM. Mixtures obtained were irritated with a halogen lamp at a photo-density of 0.25 W cm^{-2} at different time points. The absorbance intensity of ABDA at 380 nm was measured as a function of a time to determine ABDA consumption. ABDA (0.02 mM) in water, ABDA (0.02 mM) + GSH (3 mM) solutions under light illumination were used as control samples.

3.6. Heat generation of NanoP-ss-BA assemblies in a solution

NanoP-ss-BA (0.1 mM, 1 mL) and **NanoP-ss-BA** (0.1 mM, 1 mL) incubated with GSH (3 mM) were placed into the respective 10 mm quartz cuvettes. A 655 nm laser (1.5 W cm^{-2}) irradiation was then applied for 10 min. Temperature of a solutions were measured with a thermocouple equipped with a digital thermometer. MilliQ water was used as a control group.

3.7. Intracellular uptake of NanoP-ss-BA assemblies

Murine mammary gland carcinoma cells (4T1) were obtained from Seoul National University (Seoul, Korea). Cells were grown in RPMI 1640 (Roswell Park Memorial Institute) supplemented with 10% foetal bovine serum, penicillin (100 U mL^{-1}) and streptomycin (100 U mL^{-1}) and kept in 5% CO_2 at 37 °C. Cells were seeded in a 35-mm glass bottomed dishes at a density of 1 × 105 cells per dish in culture media. After overnight culture, 4T1 cells were incubated with **NanoP-ss-BA** (10 μM) for 24 h, and fluorescence images were acquired by confocal microscopy (Fluoview 1200, Olympus, Japan). Excitation light source used a 405 nm laser diode, the emission filter range was 575–675 nm, and the images were captured by 60-fold magnification with oil immersion.

3.8. Cytotoxicity assay in vitro

Cells were seeded in a 96-well plate with culture media. After overnight culture, cells were incubated with only **BA** or **NanoP-ss-BA** for 24 h and washed with DPBS. After adding new media, cells treated with **NanoP-ss-BA** were irradiated with a halogen lamp (0.19 W cm^{-2}, 15 min), and incubated for additional 24 h. To detect cell viability, MTT (Sigma) media (0.5 mg mL^{-1}) was added to the cells (treated with only **BA** or **NanoP-ss-BA)** for 4 h, the produced formazan was dissolved in DMSO (0.1 mL), and the maximum of optical density at 650 nm was read with a Spectramax Microwell plate reader.

4. Conclusion

In summary, we synthesized a new molecule (**P-ss-BA**) by conjugating the derivative **P** to the lipophilic anticancer drug **BA** through a disulphide bond. The obtained **P-ss-BA** can form stable nanoparticles in aqueous solution and maintain good stability in the physiological environment. The photoactivity of **NanoP-ss-BA** is suppressed due to AIQ. However, when exposed to a reductive environment, the cleavage of the disulphide bonds facilitated a partial disassembly of nanostructure, caused release of **P** derivatives and lipophilic anticancer drug, **BA** and restored the photoactivity of **P** derivatives. *In vitro* cell studies revealed that **NanoP-ss-BA** exhibited significant chemo- and phototoxicity against cancer cells (4T1). These results feature **NanoP-ss-BA** potential of developing stimulus responsive nanoparticles for controlled and targeted PDT of tumour. Besides it also provides a facile approach for the delivery of hydrophobic drugs.

CRediT authorship contribution statement

Zulal Özdemir: Conceptualization, Investigation, Data curation, Writing - original draft. **Mengyao Yang:** Conceptualization, Investigation, Data curation. **Gyoungmi Kim:** Investigation, Data curation. **Uladzimir Bildziukevich:** Conceptualization, Investigation, Data curation. **David Šaman:** Investigation, Data curation. **Xingshu Li:** Conceptualization, Supervision, Writing - review & editing. **Juyoung Yoon:** Funding acquisition, Supervision, Writing – review & editing, Project administration. **Zdeněk Wimmer:** Conceptualization, Funding acquisition, Supervision, Writing - review & editing, Project administration.

Declaration of competing interest

The authors declare that they have no known competing financial interests or personal relationships that could have appeared to influence the work reported in this paper.

Acknowledgements

J.Y. thanks to the support from the National Research Foundation of Korea (NRF) funded by the Korean government (MSIP) (No. 2012R1A3A2048814). Z.Ö., U. B. and Z. W. thank for funds from MPO, grants No. FV10599 and FV30300. Z.Ö. thanks the Czech Academy of Sciences grant (No. VAJVA-19-48) and University of Chemistry and Technology Prague, MOBI traineeship Programme 2019/2020 for support of her visit to the EWHA Womans University, Seoul. X.L. thanks the National Natural Science Foundation of China (Grant No. 22078066). M. Y. thanks the China Scholarship Council (CSC, No. 201904910820). The authors thank Ms. Michala Jirsová for her participation in the partial synthesis as a student.

Appendix A. Supplementary data

Supplementary data to this article can be found online at https://doi.org/10.1016/j.dyepig.2021.109307.

References

[1] Sauraj Kumar V, Kumar B, Priyadarshi R, Deeba F, Kulshreshtha A, Kumar A, Agrawal G, Gopinath P, Negi YS. Redox responsive xylan-SS-curcumin prodrug nanoparticles for dual drug delivery in cancer therapy. Mater Sci Eng C 2020;107:110356.
[2] Agostinis P, Berg K, Cengel KA, Foster TH, Girotti AW, Gollnick SO, Hahn SM, Hamblin MR, Juzeniene A, Kessel D, Korbelik M, Moan J, Mroz P, Nowis D, Piette J, Wilson BC, Golab J. Photodynamic therapy of cancer: an update. CA: Cancer J. Clin. 2011;61:250–81.
[3] Frochot C, Mordon S. Update of the situation of clinical photodynamic therapy in Europe in the 2003–2018 period. J Porphyr Phthalocyanines 2019;23:347–57.
[4] Li X, Lovell JF, Yoon J, Chen X. Clinical development and potential of photothermal and photodynamic therapies for cancer. Nat Rev Clin Oncol 2020;17:657–74.
[5] Li X, Lee S, Yoon J. Supramolecular photosensitizers rejuvenate photodynamic therapy. Chem Soc Rev 2018;47:1174–88.
[6] Xu B, Wang Z, Zhao W. Sphere–like aggregates of porphyrin as phototherapeutic agent for synergistic cancer treatment. Dyes Pigments 2021;186:108926.
[7] He Y, Liu SH, Yin J, Yoon J. Sonodynamic and chemodynamic therapy based on organic/organometallic sensitizers. Coord Chem Rev 2021;429:213610.
[8] Yang B, Chen Y, Shi J. Reactive oxygen species (ROS)-based nanomedicine. Chem Rev 2019;119:4881–985.
[9] Fan W, Huang P, Chen X. Overcoming the Achilles' heel of photodynamic therapy. Chem Soc Rev 2016;45:6488–519.
[10] Liu H, Jiang W, Wang Q, Xia J, Yu W, Wang Y, Wang Y. Microenvironment-activated nanoparticles for oxygen self-supplemented photodynamic cancer therapy. Biomater. Sci. 2020;8:370–8.
[11] Li X, Yu S, Lee D, Kim G, Lee B, Cho Y, Zheng BY, Ke MR, Huang JD, Nam KT, Chen X, Yoon J. Facile supramolecular approach to nucleic-acid-driven activatable

nanotheranostics that Overcome Drawbacks of Photodynamic Therapy. ACS Nano 2018;12:681–8.
[12] Xing P, Zhao Y. Multifunctional nanoparticles self-assembled from small organic building blocks for biomedicine. Adv Mater 2016;28:7304–39.
[13] Yang L, Zhou J, Wang Z, Li H, Wang K, Liu H, Wu F. Biocompatible conjugated porphyrin nanoparticles with photodynamic/photothermal performances in cancer therapy. Dyes Pigments 2020;182:108664.
[14] Peer D, Karp JM, Hong S, Farokhzad OC, Margalit R, Langer R. Nanocarriers as an emerging platform for cancer therapy. Nat Nanotechnol 2007;2:751–60.
[15] Mura S, Nicolas J, Couvreur P. Stimuli-responsive nanocarriers for drug delivery. Nat Mater 2013;12:991–1003.
[16] Li X, Kolemen S, Yoon J, Akkaya EU. Activatable photosensitizers: agents for selective photodynamic therapy. Adv Funct Mater 2017;27:1604053.
[17] Majumdar P, Nomula R, Zhao J. Activatable triplet photosensitizers: magic bullets for targeted photodynamic therapy. J Mater Chem C 2014;2:5982–97.
[18] Mo R, Gu Z. Tumor microenvironment and intracellular signal-activated nanomaterials for anticancer drug delivery. Mater Today 2016;19:274–83.
[19] Kennedy L, Sandhu JK, Harper ME, Culf MC. Role of glutathione in cancer: from mechanisms to therapies. Biomolecules 2020;10:1429.
[20] Yang X, Shi X, Ji J, Zhai G. Development of redox-responsive theranostic nanoparticles for near-infrared fluorescence imaging-guided photodynamic/chemotherapy of tumor. Drug Deliv 2018;25:780–96.
[21] Wang Y, Liu X, Wang X, Zheng W, Zhang J, Shi F, Liu J. Redox-responsive self-assembly PEG nanoparticle enhanced triptolide for efficient antitumor treatment. Sci Rep 2018;8:12968.
[22] Lin W, Sun T, Xie Z, Gu J, Jing X. A dual-responsive nanocapsule via disulfide-induced self-assembly for therapeutic agent delivery. Chem Sci 2016;7:1846–52.
[23] Hou W, Xia F, Alves CS, Qian X, Yang Y, Cui D. MMP2-targeting and redox-responsive PEGylated chlorin e6 nanoparticles for cancer near-infrared imaging and photodynamic therapy. ACS Appl Mater Interfaces 2016;8:1447–57.
[24] Lia L, Chen Y, Chen W, Tanc Y, Chen H, Yin J. Photodynamic therapy based on organic small molecular fluorescent dyes. Chin Chem Lett 2019;30:1689–703.
[25] Gomes ATPC, Neves MGPMS, Cavaleiro JAS. Cancer, photodynamic therapy and porphyrin-type derivatives. An. Acad. Bras. Ciênc. 2018;90:993–1026.
[26] Zhang DM, Xu HG, Wang L, Li YJ, Sun PH, Wu XM, Wang GJ, Chen WM, Ye WC. Betulinic acid and its derivatives as potential antitumor agents. Med Res Rev 2015;35:1127–55.
[27] Hordyjewska A, Ostapiuk A, Horecka A. Betulin and betulinic acid in cancer research. J. Pre-Clin. Clin. Res. 2018;12:72–5.
[28] Dai L, Li D, Cheng J, Liu J, Deng L-H, Wang L-Y, Lei J-D, He J. Water soluble multiarm-polyethylene glycol–betulinic acid prodrugs: design, synthesis, and in vivo effectiveness. Polym Chem 2014;5:5775–83.
[29] Luciano M, Brückner C. Modifications of porphyrins and hydroporphyrins for their solubilization in aqueous media. Molecules 2017;22:980.
[30] Bildziukevich U, Malík M, Özdemir Z, Rárová L, Janovská L, Šlouf M, Šaman D, Šarek J, Nonappa, Wimmer Z. Spermine amides of selected triterpenoid acids: dynamic supramolecular systems formation influences cytotoxicity of the drugs. J Mater Chem B 2020;8:484–91.
[31] Bildziukevich U, Rárová L, Šaman D, Havlíček L, Drašar P, Wimmer Z. Amides derived from heteroaromatic amines and selected steryl hemiesters. Steroids 2013;78:1347–52.
[32] Bildziukevich U, Rárová L, Šaman D, Wimmer Z. Picolyl amides of betulinic acid as antitumor agents causing tumor cell apoptosis. Eur J Med Chem 2018;145:41–50.
[33] Özdemir Z, Bildziukevich U, Šaman D, Havlíček L, Rárová L, Navrátilová L, Wimmer Z. Amphiphilic derivatives of (3β,17β)-3-hydroxyandrost-5-ene-17-carboxylic acid. Steroids 2017;128:58–67.
[34] Bildziukevich U, Rárová L, Janovská L, Šaman D, Wimmer Z. Enhancing effect of cystamine in its amides with betulinic acid as antimicrobial and antitumor agent *in vitro*. Steroids 2019;148:91–8.
[35] Steglich W, Höfle GN. *N*-Dimethyl-4-pyridinamine, a very effective acylation catalyst. Angew Chem Int Ed 1969;8:981.
[36] Bildziukevich U, Vida N, Rárová L, Kolář M, Šaman D, Havlíček L, Drašar P, Wimmer Z. Polyamine derivatives of betulinic acid and β-sitosterol: a comparative investigation. Steroids 2015;100:27–35.
[37] Bae KH, Chung HJ, Park TG. Nanomaterials for cancer therapy and imaging. Mol Cell 2011;31:295–302.
[38] Sadat S, Jahan S, Haddadi A. Effects of size and surface charge of polymeric nanoparticles on in vitro and in vivo applications. J Biomaterials Nanobiotechnol 2016;7:91–108.
[39] Hestand NJ, Spano FC. Expanded theory of H- and J-molecular aggregates: the effects of vibronic coupling and intermolecular charge transfer. Chem Rev 2018;118:7069–163.
[40] Okada S, Segawa H. Substituent-control exciton in J-aggregates of protonated water-insoluble porphyrins. J Am Chem Soc 2003;125:2792–6.
[41] Nam YS, Shin T, Park H, Magyar AP, Choi K, Fantner G, Nelson KA, Belcher AM. Virus-templated assembly of porphyrins into light-harvesting nanoantennae. J Am Chem Soc 2010;132:1462–3.
[42] Zheng X, Li Z, Chen L, Xie Z, Jing X. Self-assembly of porphyrin–paclitaxel conjugates into nanomedicines: enhanced cytotoxicity due to endosomal escape. Chem Asian J 2016;11:1780–4.
[43] Liu K, Xing R, Zou Q, Ma G, Mohwald H, Yan X. Simple peptide-tuned self-assembly of photosensitizers towards anticancer photodynamic therapy. Angew Chem Int Ed 2016;55:3036–9.
[44] Du X, Kleitz F, Li X, Huang H, Zhang X, Qiao S-Z. Disulfide-bridged organosilica frameworks: designed, synthesis, redox-triggered biodegradation, and nanobiomedical applications. Adv Funct Mater 2018;28:1707325.
[45] Feng G, Zhang G-Q, Ding D. Design of superior phototheranostic agents guided by Jablonski diagrams. Chem Soc Rev 2020;49:8179–234.